AIAA JOURNAL
Vol. 32, No. 2, February 1994

Optimization of Viscoelastic Compliant Walls for Transition Delay

Andrew E. Dixon,* Anthony D. Lucey,† and Peter W. Carpenter‡
University of Warwick, Coventry CV4 7AL, England, UK

The potential of wall compliance for delaying boundary-layer transition through the attenuation of Tollmien-Schlichting waves (TSW) has been recognized in many previous theoretical studies. The present paper seeks to determine the best transition-delaying performance possible using compliant walls made from viscoelastic materials for marine applications. The wall may take the form of either a homogeneous slab of material or a thin, stiff upper layer resting on a thick, soft substrate, the latter type holding the most promise in the practical use of compliant walls. To determine the growth rates of the TSW, a highly efficient means of solving the coupled Orr-Sommerfeld/compliant-wall eigenproblem is presented. Using spectral methods, the eigenproblem is cast in a matrix form which can then be solved using an SIMD parallel computer. What prevents the use of very soft compliant walls to suppress TSW completely is the existence of hydroelastic instabilities in the wall/flow system, namely traveling-wave flutter (TWF) and divergence. Efficient methods are also presented for the evaluation of these wall-based instabilities. A thorough investigation of the effects of the wall configuration and its material properties is carried out. Both single- and double-layer walls are optimized over the full range of wall parameters. It is shown that the best performance of single- and double-layer viscoelastic walls, respectively yield 2.5- and 5-fold delays of transition when compared with a rigid wall. These factors have been achieved using the conservative value of $n = 7$ in the e^n calculations.

I. Introduction

THE concept of using a compliant wall to postpone laminar-turbulent transition in marine applications originated with Kramer.[1,2] Substantial drag reductions, as compared with a rigid control body, were observed in tests on his compliant-coated models. There was not, however, any direct evidence that transition delay was responsible for the drag reduction. Also, the physical mechanism, proposed by Kramer to explain how wall compliance favorably affected transition, was not supported by the early theoretical studies of Benjamin,[3,4] Landahl,[5] and Landahl and Kaplan.[6] Moreover, the attempts made to corroborate Kramer's results in experimental work carried out soon after publication of his papers all ended in failure. (See a review by Bushnell and Hefner.[7]) Consequently it became a widely held view that wall compliance was not a viable method for maintaining laminar flow and, sadly, for some considerable time Kramer's pioneering work was largely dismissed.

The past ten years have seen a re-examination of Kramer's compliant-wall concept. A substantial body of theoretical and experimental work[8–20] now exists which demonstrates that wall compliance is, indeed, a viable method for transition control. The reader is referred to Riley et al.,[21] Gad-el-Hak,[22] and Carpenter[23] for reviews of this work. However, it is worth noting here that wall compliance finds practical relevance only in marine applications. For the types of wall-flow interaction necessary in this technology the densities of the two media—fluid and solid—need to be comparable. Water and rubber-type materials are well-matched and permit the construction of a robust compliant coating. In the present paper the question of whether compliant walls can be used to maintain laminar flow is regarded as settled. Accordingly we move forward to consider such issues as:

1) What limits the transition-delaying performance of a compliant wall?

2) What is the greatest possible transition delay achievable?

3) What wall properties give the best performance?

These questions have already been satisfactorily answered[11,24–26] for the plate-spring compliant wall originally introduced by Carpenter and Garrad[8] as a theoretical model of the Kramer coating. A different type of compliant wall is illustrated in Fig. 1b, comprising a soft viscoelastic substrate surmounted by a thin, much stiffer, outer layer. This type of wall was used in the experimental studies of Refs. 14–16. Such walls are simpler to manufacture than those of Kramer, and are commonly regarded as being more practical. On the other hand the theoretical modeling is considerably more involved for these two-layer walls as compared to the plate-spring type. Nevertheless the difficulties have now been overcome and an optimization study, addressing the questions posed earlier, is presented hereafter for the types of wall illustrated in Fig. 1. First, however, the physics underlying the optimization procedure will be reviewed.

Theoretical studies, including the early work of Benjamin and Landahl, show that as the wall compliance is increased the growth of the Tollmien-Schlichting waves (TSW) is progressively suppressed. In fact, if the wall were to be made sufficiently compliant the TSW would be completely stabilized, resulting in the maintenance of laminar flow for indefinitely high Reynolds numbers. Not

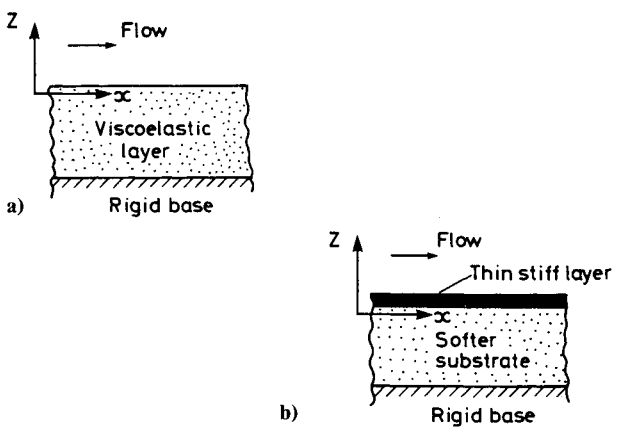

Fig. 1 Schematic of the compliant wall, a) single layer and b) double layer.

Received Feb. 12, 1993; revision received June 17, 1993; accepted for publication June 17, 1993.

*Research Fellow, Department of Engineering; currently Research Fellow, Centre for Advanced Numerical Computation in Engineering and Science, University of New South Wales, P.O. Box 1, Kensington, NSW 2033, Australia.

†Lecturer, Department of Engineering.

‡Professor of Mechanical Engineering, Department of Engineering. Member AIAA.

surprisingly this ideal situation cannot be realized in practice. The compliant wall itself is also a wave-bearing medium.[12] It supports another two classes of essentially wall-based waves, in addition to the essentially flow-based TSW. When the wall is sufficiently compliant both of these wall-based waves can develop into hydroelastic instabilities. There is also the further possibility that a wall mode and TSW coalesce to form a new, more powerful, instability. As will be explained later it is these wall-based instabilities that limit the transition-delaying performance of compliant walls.

The wall-based or hydroelastic instabilities are reviewed elsewhere,[23] so only a brief description is given here. The two types of hydroelastic instability are usually termed divergence and traveling-wave flutter (TWF). The former occurs when the conservative hydrodynamic pressure forces generated by a small disturbance on the compliant surface outweigh the restorative structural forces in the wall. The numerical simulations of Lucey and Carpenter[27,28] show this instability to take the form of a very slow downstream-traveling wave in agreement with the experimental observations of Hansen and Hunston[29,30] and Gad-el-Hak et al.[31] Furthermore, the numerical simulations confirm the view advanced by Carpenter and Garrad[9] that divergence is an absolute instability developing in both the upstream and downstream directions from the point of initiation. This implies that divergence would destroy any transition-delaying capability and must therefore be avoided.

TWF is a more subtle instability than divergence. It is convective in nature like the TSW, but travels much faster at close to the freestream speed. The instability mechanism, as first explained by Benjamin,[4] is the irreversible transfer of energy from the flow to the wall due to the work done by the fluctuating pressure. Unlike the TSW the TWF instability mechanism is essentially inviscid, although the shear flow plays a vital role. If the boundary layer were absent, leaving only unsteady potential flow, the fluctuating normal velocity and pressure at the wall would be precisely 90 deg out of phase and no irreversible energy transfer would take place. Whereas, provided that the phase speed of the wave is less than the freestream speed, the presence of a shear flow in the form of a boundary layer causes a phase shift to occur between the fluctuations in pressure and normal velocity, thereby ensuring that there will be irreversible energy transfer to the wall. The physical mechanism allows an accurate prediction to be made very simply for the onset speed of the TWF in the case of the plate-spring compliant walls.[9,32]

Like the TSW, the TWF is a convective instability. Therefore, it may well be considered that it is only necessary for its growth rate to be less than that of the TSW. It is, in fact, a far more dangerous instability than the TSW. This can be appreciated from a comparison of the neutral curves for the two types of instability shown in Fig. 2. It can be seen that for a fixed frequency the TSW only grows over a relatively narrow range of Reynolds number, whereas the growth rate of the TWF remains at a high level for an indefinitely high Reynolds number. The TWF has been shown by Lucey et al.[33] to be responsible for the very sudden onset of transition observed in some of the experiments given in Refs. 14–16. Furthermore, under certain conditions the TWF and TSW may coalesce to form a very powerful absolute instability.[8,10,20,23] Thus it is evident that the TWF must also be avoided if transition postponement is to be achieved.

Energy dissipation in the wall (or damping) was considered to be an important and beneficial property by Kramer[1,2] who carefully optimized the level of wall damping in his tests to obtain the greatest possible drag reduction. He suggested that damping acted to dissipate the energy transferred from the TSW to the wall. Benjamin[3] showed that this rather plausible explanation is, in fact, false. Damping actually leads to increased growth of the TSW. But this does not mean that damping in the wall always has a deleterious effect on transition postponement. As shown in Fig. 2, damping has opposite effects on the TSW and the TWF, that is it reduces the growth of the latter and postpones its onset to a higher Reynolds number. Furthermore, the beneficial effect on the TWF is much more pronounced than the adverse effect on the TSW. Thus, as suggested in Ref. 8, the true role of damping in the Kramer coatings was to delay the onset of TWF, thereby allowing a more compliant wall to be used. The beneficial effects of increased compliance in reducing the growth of the TSW more than offsets the detrimental effects of damping. Damping is used in this way for the optimal compliant wall designs presented later. There has been some controversy concerning the effect of damping on divergence. But numerical simulations[27] have confirmed the view advanced in Ref. 9 that the onset speed of divergence is unaffected by damping.

The first attempt at determining the compliant wall properties for obtaining the greatest transition delay was made by Gyorgyfalvy.[34] In the present paper the optimization strategy developed by Carpenter and Morris,[11] and by Carpenter[24,25] is followed. The compliant wall is required to be marginally stable with respect to divergence and TWF. This procedure results in a restricted set of optimal wall properties characterized by one or more wall parameters. These parameters are then varied to find the wall properties giving the greatest transitional Reynolds number as determined by the e^n method.

The remainder of the paper is set out as follows. The formulation of the coupled Orr-Sommerfeld/compliant-wall eigenproblem is described in Sec. II. A very large number of eigenvalues are required to implement the optimization procedure for the walls of Fig. 1b. Thus rapid solvers are all but essential. For the TSW this has been achieved by developing a Chebyshev-Tau spectral method for numerical integration of the Orr-Sommerfeld equation in a form suitable for implementation on a massively parallel SIMD computer. This method is described in the first part of Sec. III. The multideck asymptotic method of Carpenter and Gajjar[35] has been adapted for making rapid predictions of the TWF. This is described in the second part of Sec. III. The final part of this section describes the rapid methods used to predict divergence. Using these methods systematic optimization procedures are implemented for both the single-layer (Fig. 1a) and double-layer (Fig. 1b) walls and described in Sec. IV where the results are presented and discussed. Finally, the conclusions drawn from the study are given in Sec. V.

II. Formulation of the Coupled Eigenproblem

The types of wall under investigation in the present study take the form of single- or double-layer viscoelastic materials. These are illustrated in Fig. 1 together with a suitable coordinate system. The wall dynamics are modeled by the Navier equations:

$$\rho_s \frac{\partial^2 \eta_1}{\partial t^2} = G_s\left(\frac{\partial^2 \eta_1}{\partial x^2} + \frac{\partial^2 \eta_1}{\partial z^2}\right) + \left(K_s + \frac{1}{3}G_s\right)\frac{\partial}{\partial x}\left(\frac{\partial \eta_1}{\partial x} + \frac{\partial \eta_2}{\partial z}\right) \quad (1a)$$

$$\rho_s \frac{\partial^2 \eta_2}{\partial t^2} = G_s\left(\frac{\partial^2 \eta_2}{\partial x^2} + \frac{\partial^2 \eta_2}{\partial z^2}\right) + \left(K_s + \frac{1}{3}G_s\right)\frac{\partial}{\partial z}\left(\frac{\partial \eta_1}{\partial x} + \frac{\partial \eta_2}{\partial z}\right) \quad (1b)$$

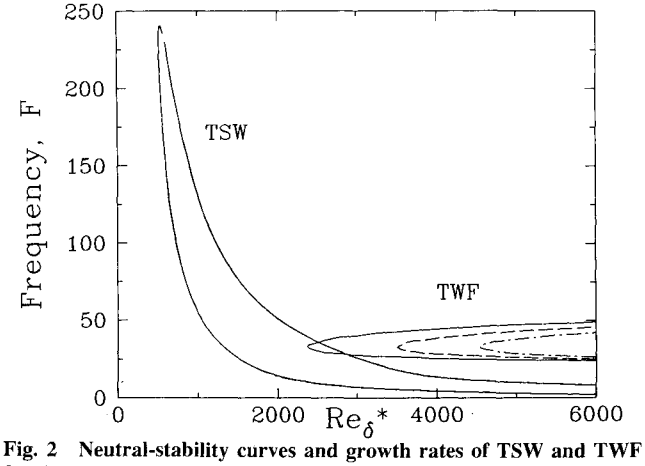

Fig. 2 Neutral-stability curves and growth rates of TSW and TWF for the double-layer wall showing the effect of substrate damping: —, $\gamma_s = 0.010$; — — $\gamma_s = 0.015$; — · — $\gamma_s = 0.020$; substrate $\bar{G}_s = 0.417$ and $\bar{d} = 1.80$. upper-layer: $\bar{E}_p = 111.1$, $\nu_p = 0.5$ and $\bar{b} = 0.1200$; flow: $Re_L = 50000$ and $\nu = 10^{-6} m^2/s$.

where x and z are, respectively, in the directions parallel and normal to the flow, (η_1, η_2) is the wall-displacement vector, ρ_s is the density of the wall material and G_s and K_s are the shear and bulk moduli defined by:

$$G_s = \frac{E_s}{2(1+\nu_s)}, \qquad K_s = \frac{E_s}{3(1-2\nu_s)}$$

with E_s and ν_s being, respectively, the elastic modulus and Poisson ratio of the material. Harmonic time variation is assumed hereafter and this permits the use of complex moduli to model viscoelastic effects. Thus, the shear modulus is written as:

$$G_s = G_{sR}(1 + i\gamma_s) \tag{2}$$

The numerical methods used would allow both the shear modulus G_{sR} and damping coefficient γ_s to be arbitrary functions of frequency. However, for simplicity, both quantities are assumed to be invariant with frequency.

Nondimensionalization, denoted by overbars, is based on the fluid density, ρ_f, flow speed, U_∞ and displacement thickness, δ^* (for distances normal to the wall). A conventional Reynolds number, Re_{δ^*}, based on the boundary-layer dispacement thickness is used to characterize the flow. Also introduced is a fixed reference Reynolds number, $Re_L = U_\infty L/\nu$, which generates a suitable length scale L for the nondimensionalization of the wall properties. It is immediately apparent that the two length scales being used herein are related through $L = \delta^*(Re_L/Re_{\delta^*})$. Thus, for example:

$$\bar{G}_s = \frac{G_s}{\rho_f U_\infty^2}, \qquad \bar{z} = \frac{z}{\delta^*} \text{ (fluid)}, \qquad \bar{z} = \frac{z}{L} \text{ (wall)}$$

$$\bar{\alpha} = \alpha\delta^*, \qquad \bar{\omega} = \frac{\omega\delta^*}{U_\infty}$$

Perturbations are assumed to take the form of a two-dimensional traveling wave with real angular frequency ω and complex wavenumber, $\alpha = (\alpha_R + i\alpha_I)$, where α_R is the wave-number and $-\alpha_I$ is the growth rate of the disturbance. Thus

$$(\eta_1, \eta_2) = \delta^*(\bar{\eta}_1, \bar{\eta}_2)\, e^{i(\alpha x - \omega t)} + \text{c.c} = \delta^*(\bar{\eta}_1, \bar{\eta}_2)\mathfrak{S} + \text{c.c} \tag{3}$$

where c.c denotes the complex conjugate. This assumption admits relatively simple solutions to the Navier equations. In the present work, wall boundary conditions require zero displacement where the layer is adhered to its rigid base so that $\bar{\eta}_1(-\bar{d}) = \bar{\eta}_2(-\bar{d}) = 0$ where d is the thickness of the compliant layer. Tangential and normal stresses due to the perturbation (η_1, η_2) are given by

$$\sigma_{21}^{(s)} = G_s\left(\frac{\partial\eta_1}{\partial z} + \frac{\partial\eta_2}{\partial x}\right) \tag{4a}$$

$$\sigma_{22}^{(s)} = 2G_s\frac{\partial\eta_2}{\partial z} + \left(K_s + \frac{1}{3}G_s\right)\left(\frac{\partial\eta_1}{\partial x} + \frac{\partial\eta_2}{\partial z}\right) \tag{4b}$$

Turning attention to the boundary-layer flow, linearization together with the assumptions of two-dimensional traveling-waves and locally parallel flow yield the Orr-Sommerfeld equation:

$$(\bar{U} - \bar{\omega}/\bar{\alpha})\,(\phi'' - \bar{\alpha}^2\phi) - \bar{U}''\phi$$

$$= (1/i\bar{\alpha}Re_{\delta^*})\,(\phi^{iv} - 2\bar{\alpha}^2\phi'' + \bar{\alpha}^4\phi) \tag{5}$$

where primes denote differentiation with respect to $\bar{z}$, the perturbation velocity is given by

$$(\bar{u}, \bar{v}) = [\phi'(\bar{z}), -i\bar{\alpha}\phi(\bar{z})]\,\mathfrak{S} + \text{c.c}$$

and $\bar{U}$ is the Blasius boundary-layer profile. The outer boundary conditions require that the perturbation velocity tends to zero. Thus

$$\phi \to 0, \qquad \phi' \to 0 \qquad \text{for } \bar{z} \to \infty \tag{6}$$

The fluid shear and normal stresses, due to the perturbation, are given by[11]

$$(\sigma_{21}^{(f)}, \sigma_{22}^{(f)}) = \rho_f U_\infty^2(\bar{\sigma}_{21}^{(f)}, \bar{\sigma}_{22}^{(f)})\,\mathfrak{S} + \text{c.c} \tag{7}$$

with

$$\bar{\sigma}_{21}^{(f)} = \frac{1}{Re_{\delta^*}}\left(\phi'' + \bar{\alpha}^2\phi + \frac{\bar{\alpha}}{\bar{\omega}}\bar{U}''\phi\right)$$

$$\bar{\sigma}_{22}^{(f)} = -\frac{1}{i\bar{\alpha}Re_{\delta^*}}\phi''' - \left(\frac{\bar{\omega}}{\bar{\alpha}} + \frac{3i\bar{\alpha}}{Re_{\delta^*}}\right)\phi' - \bar{U}'\phi + \bar{U}\phi'$$

The wall and flow solutions are coupled by imposing continuity of velocity and stress at the interface. The first of these gives at $z = 0$

$$\bar{\eta}_1 = \frac{i}{\bar{\omega}}\phi' + \frac{\bar{\alpha}}{\bar{\omega}}\phi, \qquad \bar{\eta}_2 = \frac{\bar{\alpha}}{\bar{\omega}}\phi \tag{8}$$

whereas the matching of tangential and normal stresses between wall, Eqs. (4a) and (4b), and fluid, Eq. (7), (having enforced the lower wall and outer fluid boundary conditions) can be written in the form:

$$A_{01}\phi + A_{11}\phi' + A_{21}\phi'' = \Delta_{21} \tag{9a}$$

$$A_{02}\phi + A_{12}\phi' + A_{31}\phi''' = \Delta_{22} \tag{9b}$$

where expressions for A_{ij} are given in the Appendix. For a single-layer wall, $\Delta_{21} = \Delta_{22} = 0$. However, a double-layer wall can be closely approximated by introducing a stress discontinuity, i.e., nonzero Δ_{ij}, at the interface. If the upper-layer takes the form of a thin, stiff plate, expressions for Δ_{ij} can be found using classical thin-plate theory for which the shear and normal stress contributions are found from:

$$\sigma_{21}^{(p)} = \rho_p b\frac{\partial^2\eta_{1w}}{\partial t^2} - E_p b\frac{\partial^2\eta_{1w}}{\partial x^2} \tag{10a}$$

$$\sigma_{22}^{(p)} = \rho_p b\frac{\partial^2\eta_{2w}}{\partial t^2} + B_p\frac{\partial^4\eta_{2w}}{\partial x^4} \tag{10b}$$

where (η_{1w}, η_{2w}) are the displacements of the compliant surface; E_p, ν_p, and b are, respectively, the modulus of elasticity, Poisson ratio, and thickness of the plate. B_p is the flexural rigidity of the plate which is given by:

$$B_p = \frac{E_p b^3}{12(1-\nu_p^2)}$$

Its nondimensional form is given by $\bar{B}_p = B_p/\rho_f U_\infty^2 L^3$.

Figure 3 shows that the use of this mathematical model for the mechanics of the double-layer wall (comprising a thin, stiff layer adhered to a relatively thick, soft substrate) is justified. This compares a dispersion curve for a compliant wall in vacuo, calculated using the thin-plate approximation, with that obtained from a full double-layer solution found by solving the Navier equations in each layer. The data used is representative of the types of wall used in the optimizations of Sec. IV. Also included in this figure is a single-layer compliant-wall result (obtained by simply removing the upper layer) and the result for the above plate-substrate model with the upper layer tangential stiffness, normally given by Eq. (10a), set to zero. For such walls the horizontal restraint provided by the upper layer is evidently important. It is therefore noted that the thin-plate model is a reliable approximation when the upper layer thickness is small compared to the wavelength of the disturbance.

III. Numerical and Theoretical Solution Procedures

Numerical Solution of the Orr-Sommerfeld Equation

It is necessary to integrate numerically the Orr-Sommerfeld equation (5) subject to the boundary conditions given by Eqs. (6), (8), and (9). To do this with high computational efficiency a Chebyshev-Tau method has been developed for use on a massively parallel SIMD computer. (An AMT DAP510 with 32 × 32 processors was used.) After discretization, the Orr-Sommerfeld equation is written in matrix form and becomes a nonlinear eigenvalue problem for the complex wavenumber. The eigenfunction is approximated by an Nth-order Chebyshev series:

$$\phi(z) \approx \phi_{(N)}(z) = \sum_{i=0}^{N} \hat{\phi}_i T_i[\xi(z)] = \boldsymbol{t}[\xi(z)]\hat{\boldsymbol{\Phi}} \tag{11}$$

where $\hat{\boldsymbol{\Phi}}$ is the vector of Chebyshev coefficients. The vector function $\boldsymbol{t}[\xi(z)]$ is formed from the Chebyshev polynomials, $T_i[\xi(z)]$, and $\xi(z)$ is a scaling function which maps z from the semi-infinite domain $[0, \infty)$ onto $[-1, 1]$.

Differentiation and multiplicative operations are carried out as follows. A matrix $\boldsymbol{D}$ exists[36] such that

$$\frac{d}{d\xi}\phi_{(N)}(z) = \boldsymbol{t}[\xi(z)](\boldsymbol{D}\hat{\boldsymbol{\Phi}}) \tag{12}$$

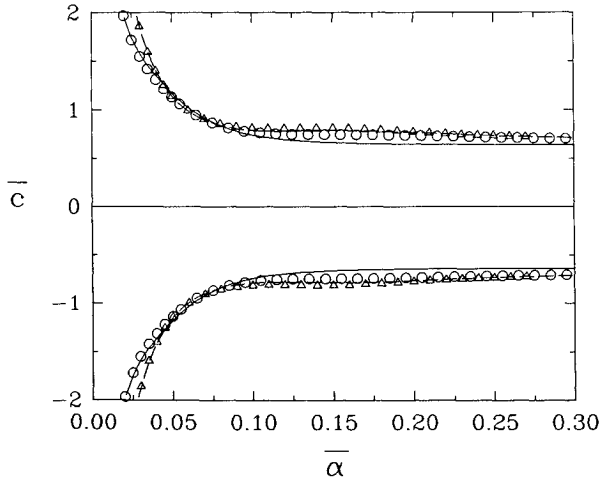

Fig. 3 Free waves for single- and double-layer compliant walls. Single-layer $\bar{E}_s$ = 1.338, ν_s = 0.49, $\bar{d}$ = 1.74 and γ_s = 0; the double-layer wall comprises a substrate with the wall and flow properties given above plus an upper layer with $\bar{E}_p$ = 118.9, ν_p = 0.5, $\bar{b}$ = 0.116, and γ_p = 0; in addition, U_∞ = 5.8; m/s and δ^* = 0.431; mm have been used for nondimensionalization; ———, single-layer wall; O, double-layer wall with upper-layer horizontal stiffness suppressed; — — double-layer wall; Δ, full double-layer wall solution.

That is, the derivative of a Chebyshev series can be found by premultiplying the vector of Chebyshev coefficients by the matrix $\boldsymbol{D}$. Furthermore, the product of two Chebyshev series $f_{(N)}(\xi)$ and $\phi_{(N)}$ can be expressed as:

$$f_{(N)}(\xi)\phi_{(N)} \approx \boldsymbol{t}(\xi)(\boldsymbol{F}\hat{\boldsymbol{\Phi}}) \tag{13}$$

where $\boldsymbol{F}$ is a $(N+1) \times (N+1)$ matrix dependent on the elements of the Chebyshev coefficients of $f_{(N)}(\xi)$ and is termed the product matrix of $f_{(N)}(\xi)$. The derivative matrix with respect to z can then be expressed as:

$$\boldsymbol{D}_z = \boldsymbol{W}\boldsymbol{D} \tag{14}$$

having used the chain rule and where $\boldsymbol{W}$ is the product matrix of the Chebyshev decomposition of $d\xi/dz$ in terms of $T_i[\xi(z)]$. The higher derivatives, $\boldsymbol{D}_z^i$ (i = 2, 3...), are similarly found.

It is now possible to reduce the Orr-Sommerfeld equation to the analogous matrix equation:

$$\boldsymbol{M}(\bar{\alpha}; \bar{\omega}, Re_{\delta^*})\hat{\boldsymbol{\Phi}} = 0 \tag{15}$$

where

$$\boldsymbol{M}(\bar{\alpha}; \bar{\omega}, Re_{\delta^*}) = [\boldsymbol{I}]\bar{\alpha}^4 + [iRe_{\delta^*}\boldsymbol{U}]\bar{\alpha}^3 - [2\boldsymbol{D}_z^2 + iRe_{\delta^*}\bar{\omega}\boldsymbol{I}]\bar{\alpha}^2$$

$$+ [iRe_{\delta^*}(\boldsymbol{E} - \boldsymbol{U}\boldsymbol{D}_z^2)]\bar{\alpha} + [\boldsymbol{D}_z^4 + iRe_{\delta^*}\bar{\omega}\boldsymbol{D}_z^0] \tag{16}$$

The matrices $\boldsymbol{U}$ and $\boldsymbol{E}$ are, respectively, the product matrices of the Chebyshev decomposition of the boundary-layer velocity profile, $\boldsymbol{U}$, and its second derivative, $\boldsymbol{U}''$. The corresponding vectors of Chebyshev coefficients are denoted by $\hat{\boldsymbol{u}}$ and $\boldsymbol{D}_z^2\hat{\boldsymbol{u}}$. All of the matrices on the right-hand side of Eq. (16) can be assembled directly and stored. On a SIMD machine, the matrix $\boldsymbol{M}(\bar{\alpha}; \bar{\omega}, Re_{\delta^*})$ can then be found efficiently, for different values of its arguments, using parallel addition.

To implement the interfacial boundary-conditions the *Tau* method was chosen. The operations described above can be used to find the discretized form of the boundary conditions. For example, Eq. (9) becomes:

$$(\boldsymbol{A}_{01}\boldsymbol{d}_0 + \boldsymbol{A}_{11}\boldsymbol{d}_1 + \boldsymbol{A}_{21}\boldsymbol{d}_2)\hat{\boldsymbol{\Phi}} = 0$$

$$\text{where} \quad \boldsymbol{d}_i = \boldsymbol{t}[\xi(0)]\boldsymbol{D}_z^i \quad (i = 0, 1, 2) \tag{17}$$

for the single-layer case. The vectors $\boldsymbol{d}_i$ are evaluated first and stored, making it possible to update the boundary conditions for different $\boldsymbol{A}_{ij}$ efficiently using vector addition. The outer boundary conditions, Eq. (6), become:

$$\boldsymbol{t}[\xi(\infty)]\hat{\boldsymbol{\Phi}} = 0 \tag{18a}$$

$$\boldsymbol{t}[\xi(\infty)]\boldsymbol{D}_z^0\hat{\boldsymbol{\Phi}} = 0 \tag{18b}$$

The four boundary conditions replace the last four rows of the matrix $\boldsymbol{M}$.

The algebraic mapping from the physical to the computational domains is:

$$\frac{z}{h} = \frac{1+\xi}{1-\xi} \tag{19}$$

where the value of h was selected for greatest accuracy. In consequence, Eq. (18b) is automatically satisfied, thus requiring a stronger condition to be imposed. Since the solutions decay exponentially in this region it can be shown that as $z \to \infty$, $\phi_\xi \to 0$. This is then taken as the second outer boundary condition.

For a given Re_{δ^*} and $\bar{\omega}$, Eq. (15) is a nonlinear eigenvalue problem for $\bar{\alpha}$. In the rigid-wall case, $\boldsymbol{M}$ takes the form of a polynomial in $\bar{\alpha}$ with matrix coefficients which can be solved globally. When a one- or two-layer compliant wall is introduced it takes the form of a transcendental equation for $\bar{\alpha}$ making a global solution impossible. Thus a local iterative method must be used. The procedure, derived by Bridges and Morris[37] is defined by:

$$\bar{\alpha}_{k+1} = \bar{\alpha}_k - 1/Tr\{\boldsymbol{M}^{-1}(\bar{\alpha}_k)\boldsymbol{M}_{\bar{\alpha}}(\bar{\alpha}_k)\} \tag{20}$$

where $Tr\{\}$ denotes the trace of the matrix enclosed in the brackets and $\boldsymbol{M}_{\bar{\alpha}}$ is the derivative of $\boldsymbol{M}$ with respect to $\bar{\alpha}$. For convenience, reference to the other parameters has been dropped. All the operations in Eq. (20) can be carried out efficiently on a parallel machine. The derivative was found analytically for the Orr-Sommerfeld terms and numerically for the boundary-condition terms.

With 31 modes included in the Chebyshev expansion, accuracy to four decimal figures was attained for the eigenvalue of the Tollmien-Schlichting mode for the rigid-wall case. These results showed good agreement with those of Jordinson.[38] For the case of compliant-wall boundary conditions, 40–48 modes were necessary to achieve the same accuracy. These results agreed favorably with those of Yeo.[39] For the TWF mode, 63 modes were necessary. This more severe requirement is due to the fact that the TWF eigenfunction decays on a shorter length scale than that of the boundary-layer thickness, thereby requiring more collocation points to describe it accurately.

In the compliant-wall calculations, the radius of convergence was found to be very small. At least two significant figures were necessary for the initial estimate before convergence was obtained. However, the computational efficiency of the method renders it a powerful tool for the repeated calculation of eigenvalues undertaken for the wide range of wall parameters considered in the optimization procedures of Sec. IV.

Asymptotic Method for Predicting Traveling-Wave Flutter

The evaluation of TWF behavior can be carried out by solving the Orr-Sommerfeld equation using the methods presented above. Despite their efficiency, the use of these methods can be computationally expensive when predicting TWF because faster alternative methods are available. The onset of TWF occurs when the phase speed of the surface wave is very close to the freestream flow speed.[32] Consequently, solutions to the Orr-Sommerfeld equation for this mode can be very difficult to locate and track, possibly due to problems associated with the continuous spectrum. In many of the cases studied here, then, it is only practical to use the following method of TWF prediction.

The flow solution is obtained from Carpenter and Gajjar[35] and adapted for the present types of compliant walls. They used a multideck approach to obtain a general asymptotic solution to the linearized Navier-Stokes equations for a boundary layer over a compliant wall. The boundary-layer structure is modeled by a viscous wall layer, an inviscid shear layer, and an outer potential flow. This is a high-Reynolds-number asymptotic solution which additionally assumes long-wavelength disturbances, i.e., small $\bar{\alpha}$. In the following, the phase speed, $c = \omega/\alpha$, is introduced and subsequently all wave speeds are nondimensionalized using U_∞. The nondimensional amplitudes of the tangential and normal fluid stresses at the wall/flow interface take the forms:

$$\bar{\sigma}_{21}^{(f)} = \bar{\alpha}[T_h\bar{\eta}_{1w} + T_v\bar{\eta}_{2w}] \tag{21a}$$

$$\bar{\sigma}_{22}^{(f)} = \bar{\alpha}[P_h\bar{\eta}_{1w} + P_v\bar{\eta}_{2w}] \tag{21b}$$

where

$$T_h = \varepsilon\bar{\alpha}^{1/2}C_{m2}\bar{c}^{3/2}(1+i)/\sqrt{2} \tag{22a}$$

$$T_v = \bar{\varepsilon}\alpha^{1/2}C_{m2}(1-\bar{c})^2(-1+i)/\sqrt{2\bar{c}} \tag{22b}$$

$$P_h = -\varepsilon\bar{\alpha}^{1/2}C_{m2}(1-\bar{c})^2(1-i)/\sqrt{2\bar{c}} \tag{22c}$$

$$P_v = C_{m2}(1-\bar{c})^2 + \bar{\alpha}C_{m2}\left\{2\bar{c} - \frac{1}{H} - (1-\bar{c})^2\Phi_\infty(\bar{c})\right\}$$

$$-\varepsilon\bar{\alpha}^{1/2}C_{m2}\frac{(1-\bar{c})^4}{\bar{c}^{5/2}}\frac{(1+i)}{\sqrt{2}} \tag{22d}$$

C_{m2} is the ratio of fluid-to-substrate densities, H is the boundary-layer shape parameter ($H = 2.591$ for the Blasius profile) and $\Phi_\infty(\bar{c})$ is a known complex function which is assumed (in this application) to be dependent only on the real part of the complex phase speed. Interpolation functions for $\Phi_\infty(\bar{c})$ are given in Ref. 35. The small parameter, $\varepsilon = 1/\sqrt{Re_{\delta^*}}$, follows from the scalings in the multideck structure.

The first term on the right-hand side of Eq. (22d) represents the contribution from the purely potential flow outside the boundary layer which gives pressures exactly in phase with vertical displacements of the wall. The second term accounts for the inviscid shear layer; this applies a phase shift to the otherwise conservative forces through the complex function, Φ_∞. It is this phase shift to the pressure which allows the irreversible energy transfer from the flow into the wall that can lead to TWF. The third term in Eq. (22d) together with all of Eqs. (22a–22c) account for the effect of the viscous wall layer. These terms also provide a mechanism for irreversible energy transfer between the flow and the wall. Whether or not TWF occurs depends on the balance of all of these rates of wall/flow irreversible energy transfer and the rate of dissipation of wall energy through damping. A fuller account of the various energy-transfer mechanisms is given in Refs. 11 and 23.

The usefulness of this flow solution can be seen from Eqs. (21): the fluid stresses are written as linear combinations of the wall perturbations. Thus, the solution for the complete wall/flow system reduces to merely solving the wall equations subject to four boundary conditions, namely continuity of wall/fluid stresses at the interface and zero displacement at the bottom of the compliant-wall layer. Following the methods of Duncan, Waxman, and Tulin,[12] the Helmholtz decomposition is used to write the displacement vector, (η_1,η_2), as a sum of its rotational and irrotational parts. Solutions of the Navier equations, (1), can then be found by considering a pair of second-order differential equations. By assuming traveling-wave disturbances, these admit simple solutions and the reconstituted nondimensional disturbance vector is then found to have the amplitude components

$$\bar{\eta}_1 = i\bar{\alpha}\sinh(\bar{\alpha}K_L l\bar{z})A_1 + i\bar{\alpha}\cosh(\bar{\alpha}K_L l\bar{z})A_2$$

$$+\bar{\alpha}K_T\cosh(\bar{\alpha}K_T l\bar{z})A_3 + \bar{\alpha}K_T\sinh(\bar{\alpha}K_T l\bar{z})A_4 \tag{23a}$$

$$\bar{\eta}_2 = \bar{\alpha}K_L\cosh(\bar{\alpha}K_L l\bar{z})A_1 + \bar{\alpha}K_L\sinh(\bar{\alpha}K_L l\bar{z})A_2$$

$$-i\bar{\alpha}\sinh(\bar{\alpha}K_T l\bar{z})A_3 - i\bar{\alpha}\cosh(\bar{\alpha}K_T l\bar{z})A_4 \tag{23b}$$

where $l = Re_L/Re_{\delta^*}$ and

$$K_T^2 = 1 - (\bar{c}/\bar{c}_T)^2, \qquad K_L^2 = 1 - (\bar{c}/\bar{c}_L)^2$$

The dimensional transverse and dilational wave speeds in the solid are given by

$$c_T = \sqrt{\frac{G_s}{\rho_s}}, \qquad c_L = \sqrt{\frac{K_s}{\rho_s} + \frac{4G_s}{3\rho_s}}$$

In Eq. (23), A_i ($i = 1, 2, 3, 4$) are constants of integration which can be determined by imposing boundary conditions. The requirement of zero displacement at $\bar{z} = -\bar{d}$ provides two of these, the other two are obtained from Eqs. (4a) and (4b) in the following way. At the top of the wall layer, the stresses in the solid are found by introducing Eqs. (23a) and (23b) into the non-dimensional form of Eqs. (4a) and (4b). These are then equated to the fluid stresses which are obtained from substituting Eqs. (23a) and (23b) into Eqs. (21a) and (21b). When a thin upper wall layer is present, a discontinuity of stresses is introduced at the interface as discussed in Sec. II. The enforcement of these four boundary conditions yields a linear system of equations (of order 4) for the unknowns, A_i. In matrix form it is described by:

$$\boldsymbol{Sa} = 0 \tag{24}$$

where $\boldsymbol{a}$ is the vector of the coefficients, A_i. The stipulation of non-trivial solutions yields the eigenvalue problem:

$$\det[\boldsymbol{S}(\bar{\alpha}; \bar{c}, Re_{\delta*})] = 0 \tag{25}$$

This has been solved numerically using the method of false position. In the formulation given above either spatially growing waves ($\bar{\alpha}$ complex, $\bar{\omega}$ real) or temporally growing waves ($\bar{c}$ complex, $\bar{\alpha}$ real) can be assumed. The latter form is more convenient for computing the TWF and has been used for the present work. Both forms, of course, give the same results for neutral stability. Further details of the above procedures, together with a listing of the elements of $\boldsymbol{S}$, are given by Lucey et al.[33]

The method described previously has been compared with numerical solutions of the Orr-Sommerfeld equation for a variety of cases. Provided that the condition of small $\bar{\alpha}$ is adhered to, good agreement is found with a tendency for the asymptotic method to produce slightly pessimistic estimates of instability. In the context of compliant-wall design, this type of disparity is acceptable.

Divergence Prediction

It has been shown by Lucey and Carpenter[27] that divergence instability first occurs at the flow speed for which a formerly upstream-traveling surface wave turns to travel downstream under the influence of the hydrodynamic forces. Onset can therefore be considered to occur at the flow speed for which $\bar{c}$ first becomes zero at some critical wavenumber. Figure 4 shows an identical dispersion curve to Fig. 3 except that a fluid flow has been included. The flow speed is just below that at which divergence occurs; note that the upstream branch comes very close to $\bar{c}_R = 0$ at $\bar{\alpha} \approx 0.1$. In the absence of damping, this branch has neutral stability ($\bar{c}_I = 0$) throughout the wavenumber range. Potential flow has been assumed to generate this result. This gives somewhat pessimistic predictions, since Kendall[40] and Balasubramanian and Orszag[41] indicate that a scaling factor (less than unity) should be applied to the hydrodynamic forces to account for the effect of a boundary layer. Also included in Fig. 4 is the dispersion curve for the downstream-traveling wave, calculated from the asymptotic flow solution. Note that TWF is occuring for wavenumbers in the range 0.07–0.23. Thus, for this undamped wall TWF is the critical wall instability. However, the TWF could be eliminated by introducing less than 1% damping. If this were done and the flow speed were marginally increased then divergence would become the critical instability since its onset remains unaffected by damping.

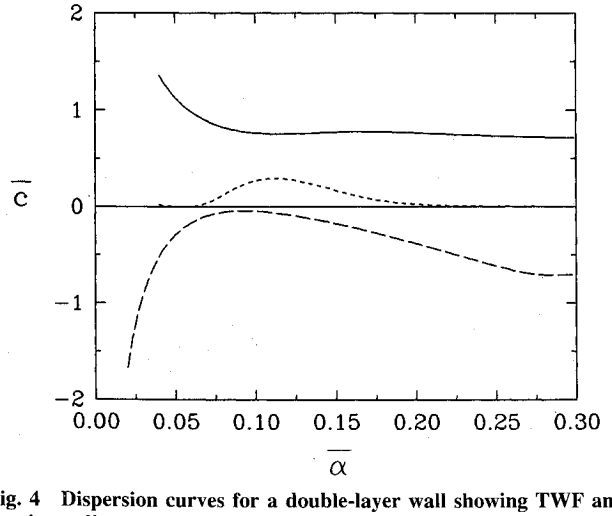

Fig. 4 Dispersion curves for a double-layer wall showing TWF and imminent divergence onset; All data as for Fig. 2; fundamental downstream-traveling wave, asymptotic flow solution: ———, c_R; — — —, $c_I \times 100$; fundamental upstream-traveling wave, potential flow: — —, c_R; $c_I = 0$ throughout.

The exact flow speed U_d at which divergence instability first occurs can be found analytically upon consideration of Fig. 4. The value of U_∞ for which the upstream branch first intersects $c_R = 0$ is found. Assuming potential flow, then $T_h = T_v = P_h = 0$ and $P_v = C_{m2}(1 - \bar{c})^2$ in Eqs. (22) and the dimensional form of the dispersion relation, Eq. (25), can be expanded. For a double-layer compliant wall, the appropriate divergence onset flow speed for a given wavenumber is found by taking the limit $c \to 0$. Thus

$$\rho_f U_d^2 = 2G_s W(\alpha d, \kappa) + (\alpha b)^3 B_p \tag{26}$$

where $\kappa = c_T^2/c_L^2$ and the function W is defined by

$$W \equiv \frac{1 + (\alpha d)^2(1 + \kappa^2) + (1 - \kappa^2)\sinh^2(\alpha d)}{(1 + \kappa)\sinh(\alpha d)\cosh(\alpha d) - (1 - \kappa)(\alpha d)}$$

Note that in the limit of an incompressible substrate, $\kappa \to 0$ and thus $W \equiv W(\alpha d)$. The right-hand side of Eq. (26) can be evaluated for a range of values of α to find the minimum value of U_d and the wavenumber of the critical divergence mode.

For a single-layer wall, the above result can be used with $B_p = 0$. However, the function W monotonically decreases with increasing α. Thus, the lowest divergence onset speed is found where $\alpha \to \infty$ (i.e., the critical mode has zero wavelength) with $W \to 1$ and gives that

$$\rho_f U_d^2 = 2G_s \tag{27}$$

In contrast to the double-layer result, Eq. (26), this prediction is very unsatisfactory since there is no dependence on the depth of the layer. The experimental work of Gad-el-Hak et al.[31] clearly showed that U_d depends on the depth of the viscoelastic layer, as might be expected on physical grounds because thicker layers are more compliant. Furthermore, a finite critical wavenumber exists which depends upon both the wall thickness and its shear modulus. These features are present in the double-layer wall which may be regarded as a resonant wall which has "preferred" modes. The single-layer wall behavior is not fully understood but the assumption of an infinitely long wall may underlie the present findings. Lucey and Carpenter[42] have shown that the constraint of finiteness provides a second restorative component to flexible walls of a single structural component thereby making them *resonant*. The recent theoretical work of Werle et al.[43] in which the hydroelastic stability of a single-layer finite compliant panel is studied using the finite-element method has shown the dependence of U_d on the wall thickness. However, at present, these numerical methods are far less convenient than the simple analytical expressions of Eqs. (26) and (27). Thus, the results of Eqs. (26) and (27) will be used in the knowledge that they provide conservative estimates of divergence-onset flow speeds.

IV. Optimization Procedure and Results

Empirical evidence[44] suggests that the linear regime of transition ends when the local amplitude of the disturbance has grown to approximately e^7 times its initial amplitude. Further downstream of the linear region, nonlinear effects become important and the flow disturbances take on a three-dimensional character. Shortly

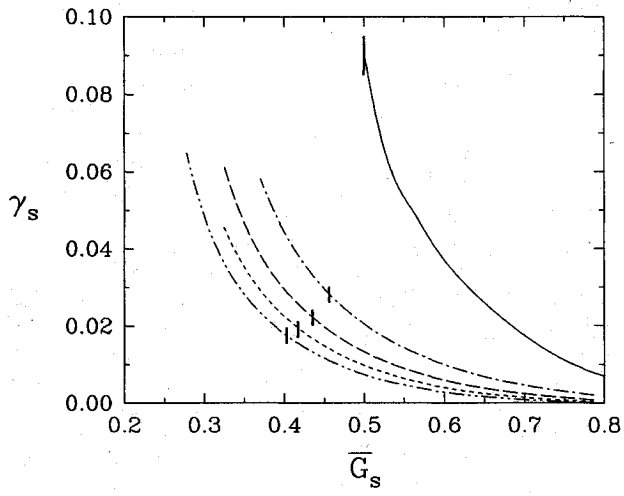

Fig. 5 Variation of wall damping with substrate shear modulus which gives marginal stability with respect to TWF for various upper layers: ——— single-layer wall (complete elimination of TWF), double-layer walls (TWF first occurs at $Re_{\delta*}$ = 3600): — · —, $\bar{b}$ = 0.00534; — —, $\bar{B}_p$ = 0.01067; — — —, $\bar{B}_p$ = 0.01602; — · · —, $\bar{B}_p$ = 0.02136. Other data: $\bar{d}$ = 1.80, $\bar{b}$ = 0.1200, ν_p = 0.5, Re_L = 50,000 and $\nu = 10^{-6} m^2/s$. The thick vertical lines indicate the minimum value of $\bar{G}_s$ (for each $\bar{B}_p$ line) required to prevent divergence.

after, the transition to turbulence takes place. For the flat-plate boundary layer the linear regime represents some 80% of the total transition region. It is therefore here that substantial benefits can be gained by reducing the growth rate of the TSW mode in order to delay transition.

The e^n method of Smith and Gamberoni[44] for transition prediction is used as follows. Knowing the growth rates in the region of instability, the amplitude of a TSW with a given frequency can be calculated as a function of the Reynolds number from

$$a_f/a_i = \exp\left\{-\int_{x_i}^{x_f} \alpha_I \, dx\right\} \tag{28}$$

in which a_f is the amplitude at downstream location, x_f, where the Reynolds number is $Re_{\delta*}$ and a_i is the initial amplitude at x_i, which is taken to be at the lower branch of the neutral curve. The integral is taken along a path such that the frequency parameter F ($F \equiv \bar{\omega} \times 10^6/Re_{\delta*}$) is kept constant. F is made dimensionless in such a way as to be invariant with respect to boundary-layer scalings and, thus, distance along the plate. The lowest Reynolds number for which $a_f/a_i = e^7$ can therefore be found by performing the previous calculations over a range of values of F. In practice, a set of 6 to 10 frequencies is generally adequate. The Reynolds number determined in this way can be regarded as the limit of the linear regime of transition.

For all of the following results, we have assigned the reference Reynolds number, Re_L, a value of 50,000 and have used a kinematic viscosity, $\nu = 10^{-6}$ m^2/s. To quantify the performance of a compliant wall a transition-delay factor (TDF) is introduced. Following Gyorgyfalvy,[34] it is defined by

$$\text{TDF} = \left\{ \frac{[(Re_{\delta*})_{e^7}]_{\text{compliant wall}}}{[(Re_{\delta*})_{e^7}]_{\text{rigid wall}}} \right\}^2 \tag{29}$$

where $(Re_{\delta*})_{e^7}$ is the Reynolds number for which $\max(a_f/a_i) = e^7$. The TDF yields a comparative measure of the distance from the leading edge to the transition point.

It should be noted that the use of $n = 7$ in the e^n method, rather than the usual value of 9–10, is very conservative. Essentially, our estimates of transitional Reynolds number are based on the limit of the linear regime of transition. This conservative choice for n was made because the effects of wall compliance in the nonlinear regime of transition are relatively unexplored. All such recent studies,[19,45–47] however, indicate that wall compliance maintains its beneficial effect well into the nonlinear regime. This suggests that we would have been justified in using n = 9.5, say; in which case the substantial transition delays obtained would have been even greater.

The wall properties are sought which give the largest possible value of TDF. This search is carried out under the constraint that no other unstable modes (TWF or divergence) are present which might cause the transition to turbulence by an alternative mechanism. As discussed in Refs. 8 and 9, the effects of increasing the wall stiffness (achieved here by raising the shear modulus of the lower layer and/or increasing the flexural rigidity of the upper layer), decreasing the wall inertia or increasing the wall damping tend to stabilize the TWF mode but increase the growth rates of the TSW mode. Typical F-$Re_{\delta*}$ plots of neutral-stability curves for a double-layer wall showing the effect of substrate damping are presented in Fig. 2. For reasons given previously the optimal compliant wall must be marginally stable with respect to TWF. This could be achieved by incorporating sufficient damping in the wall in order to increase the critical Reynolds number for the TWF, so that it is either effectively infinite or, at least, corresponds to the trailing edge of the compliant panel. It must also be ensured that the wall is not unstable to divergence.

Optimization of the Single-Layer Viscoelastic Wall

For an incompressible single-layer compliant wall there are three wall parameters which can be varied when conducting the search for maximum transition delay, namely, wall depth, shear modulus, and damping. It is assumed that the density of the wall is the same as the fluid. Soft compliant walls are unstable with respect to TWF. As the shear modulus is increased, the growth rate of this instability decreases as does the size of the domain of instability in the F-$Re_{\delta*}$ plane. A further rise in the shear modulus causes the domain of instability to vanish rapidly, at least for all the Reynolds numbers investigated (≤10,000). For a given substrate depth, the minimum value of the damping coefficient required to eliminate the TWF has been plotted against the shear modulus as the solid line in Fig. 5. Note that to maintain marginal stability for the TWF, a reduction in shear modulus must be accompanied by increased wall damping. This curve has been found to be largely independent of the wall thickness. The e^n-type calculations for the TSW mode were investigated along this marginal-stability curve. For a given substrate depth, a series of plots were made of the logarithm of the TSW amplitude ratio, $\ell_n(a_f/a_i)$, for a range of frequencies. From these results, an envelope of maximum amplification (against the Reynolds number) can be determined. Such envelopes are presented in Fig. 6a for various values of shear modulus.

From Fig. 6a it can be seen that the largest local amplitude ratio for a given Reynolds number occurs for the rigid-wall case (i.e., infinite $\bar{G}_s$). As the shear modulus is reduced (and the level of damping increased) the local amplitude ratio decreases uniformly for all Reynolds numbers until a minimum is reached. The smallest growths are found for the combination of $\bar{G}$ = 0.55 with γ_s = 0.05. A further reduction in the shear modulus causes the local amplitude to rise again. The reason for this is that the adverse effect on the TSW of the relatively high damping necessary for the stabilization of the TWF mode when the wall is very soft outweighs the beneficial effect of increased compliance.

The results discussed above correspond to a fixed wall depth. Provided that the wall depth is much greater than the longest TSW wavelength of interest, the compliance will be identical to that of an infinitely deep wall. A wall depth of $\bar{d}$ = 1.60 meets this criterion. But also plotted in Fig. 6a is the maximum amplification envelope for $\bar{d}$ = 0.80 with zero damping. If this curve is compared with the curve corresponding to $\bar{d}$ = 1.60 with zero damping (the solid line), it will be observed that the two curves coincide at low Reynolds numbers where the TSW wavelengths are relatively

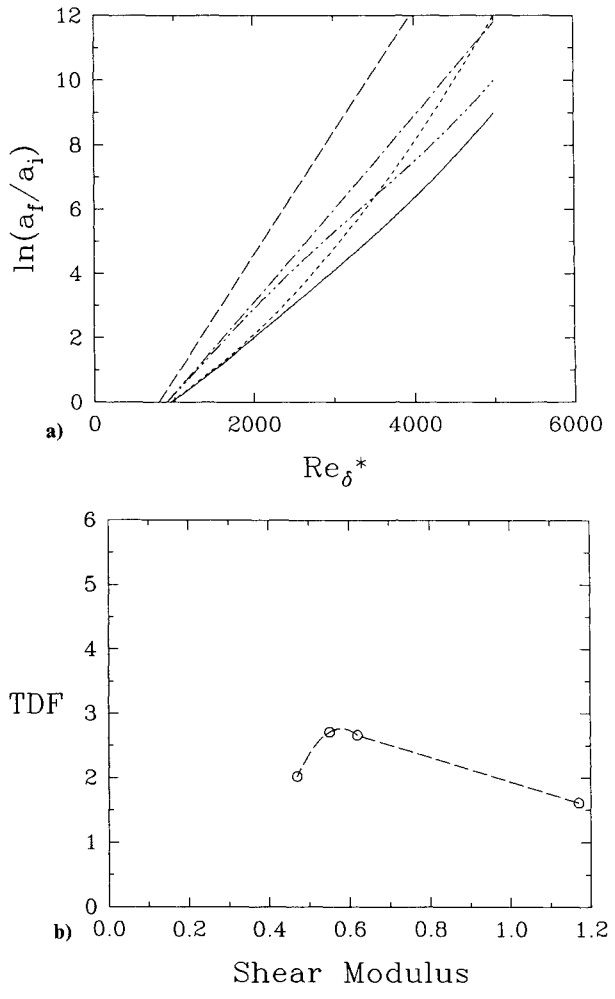

Fig. 6 *Results of* e^7 **calculations for TSW over a single-layer compliant wall. In each case the wall is stable with respect to TWF for all** $Re_{\delta*}$**: a) Maximum amplification envelopes — — —, rigid wall; — · —,** $\bar{G}_s = 1.17$, $\gamma_s = 0$, $\bar{d} = 1.60$; **— · · —,** $\bar{G}_s = 0.55$, $\gamma_s = 0.05$, $\bar{d} = 1.60$; **— — —,** $\bar{G}_s = 0.47$, $\gamma_s = 0.1$, $\bar{d} = 1.60$; **— — —,** $\bar{G}_s = 0.55$, $\gamma_s = 0$, $\bar{d} = 0.80$. **b) The variation of TDF with shear modulus.**

small, but diverge at higher Reynolds numbers where the wavelengths are relatively large. It is also evident that, as expected, greater transition delay is obtained using the thicker $\bar{d} = 1.60$ wall, the depth of which is effectively infinite.

Divergence instability must also be considered. In the case of the single-layer compliant wall, use of Eq. (27) shows that divergence onset does not occur until $\bar{G} = 0.5$. The optimal value of $\bar{G}$ found above is greater than this. The transition-delaying performances of the above single-layer walls, based on the e^7 criterion, are summarized in Fig. 6b from which the maximum value of TDF = 2.5 is found. Thus, for the best single-layer wall the onset of transition occurs at a Reynolds number of 4300, as compared with the rigid-wall value of 2700.

Optimization of the Double-Layer Wall

The double-layer wall is a much more complex case to optimize because there is a larger number of wall parameters which can be varied; thus, much greater computational effort is required. In addition to varying the substrate parameters (discussed earlier for the single-layer wall), the thickness, elastic modulus, and damping of the upper-layer flexible plate can also be varied. In the following it is assumed that the flow, substrate, and plate densities are identical.

For a given upper layer, the asymptotic method discussed in Sec. III is used to determine the variation of substrate damping with shear modulus (for a given substrate depth) which is required to postpone the onset of TWF until a prescribed Reynolds number is reached. Typical results for four different upper layers are plotted in Fig. 5. These double-layer results were obtained by finding the wall properties which placed the critical Reynolds number for TWF at 3600. The divergence characteristics (which are independent of damping) were also considered. Using Eq. (26), the values of $\bar{G}_S$ corresponding to the onset of divergence were calculated and are denoted by the thick vertical lines in Fig. 5. These are the minimum permissible shear moduli for each wall configuration. The local amplitudes of the TSW were calculated at points along each curve of Fig. 5 excluding the regions where divergence existed. Sample maximum amplification envelopes for three points along one of the $\bar{B}_p$ curves in Fig. 5 are presented in Fig. 7.

For low values of the Reynolds number (up to $Re_{\delta*} \approx 2200$), the local amplitudes of the TSW are almost identical to those of a rigid wall. However, at higher Reynolds numbers, all three curves show a reduction in amplitude compared to the rigid wall. The reason for this Reynolds number dependence can be explained as follows. Substituting the form of Eq. (3) into Eqs. (10), it can be seen that

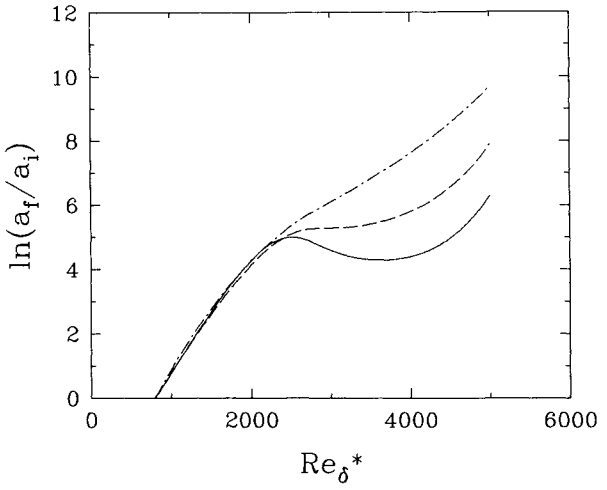

Fig. 7 Maximum amplification envelopes for the TSW over double-layer walls having a fixed upper layer with different substrate shear moduli; in each case the wall is stable with respect to TWF up to $Re_{\delta*} = 3600$: **— · —,** $\bar{G}_s = 0.787$, gs = 0.002; **— —,** $\bar{G}_s = 0.574$, $\gamma_s = 0.011$; **——— —,** $\bar{G}_s = 0.463$, $\gamma_s = 0.023$. **Other data:** $\bar{d} = 1.80$, $\bar{B}_p = 0.01067$, $\bar{b} = 0.1910$, **and** $\gamma_p = 0$.

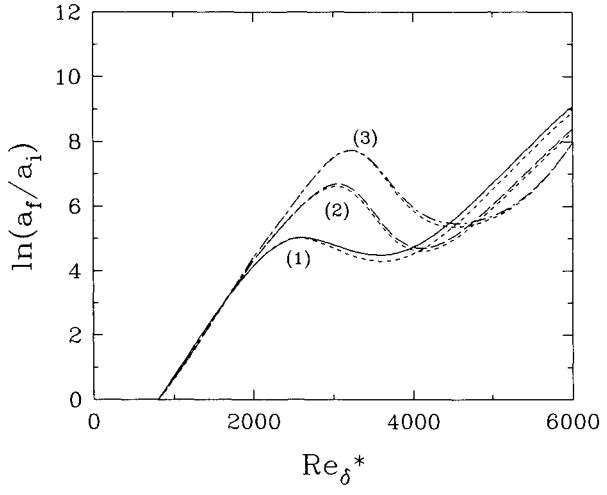

Fig. 8 Effect of upper-layer stiffness on the maximum amplification envelopes for TSW; in each case the wall is stable with respect to TWF up to $Re_{\delta*} = 5700$ **and is marginally stable for divergence;** $\bar{d} = 1.8$ **and** $\gamma_p = 0$ **throughout: 1)** $\bar{B}_p = 0.01067$: ——— $\bar{G}_s = 0.435$, $\gamma_s = 0.0375$, $\bar{E}_p = 55.6$, $\bar{b} = 0.1200$; ——— $\bar{G}_s = 0.435$, $\gamma_s = 0.0306$, $\bar{E}_p = 277.8$, **and** $\bar{b} = 0.0702$. **2)** $\bar{B}_p = 0.02131$: — — $\bar{G}_s = 0.403$, $\gamma_s = 0.0296$, $\bar{E}_p = 111.0$, $\bar{b} = 0.1200$; ——— $\bar{G}_s = 0.403$, $\gamma_s = 0.0264$, $\bar{E}_p = 277.8$, **and** $\bar{b} = 0.0880$. **3)** $\bar{B}_p = 0.03200$: — · — $\bar{G}_s = 0.380$, $\gamma_s = 0.0254$, $\bar{E}_p = 166.7$, $\bar{b} = 0.1200$; ——— $\bar{G}_s = 0.380$, $\gamma_s = 0.0254$, $\bar{E}_p = 277.8$, **and** $\bar{b} = 0.0101$.

the normal and tangential stiffness contributions (arising from the second terms on the right-hand sides of each equation) of the upper layer are respectively proportional to $\alpha(\alpha b)^3$ and $\alpha(\alpha b)$. Now, for a given Reynolds number, the value of the local amplitude is dictated by the frequencies which are unstable for that Reynolds number. At low Reynolds numbers, the higher frequencies of the TSW, where the wavenumber is large, determine the stability envelope. Thus the upper layer, with the dependence mentioned above, "appears" to be very stiff and behaves very much like the rigid wall. However, at a higher Reynolds number, the frequencies of the TSW instability become lower, giving lower wavenumbers and hence a more compliant upper layer. At even higher Reynolds numbers the local amplitudes once more show a rapid increase. This is due to substrate effects. At the lower wavenumbers (associated with the high Reynolds numbers), the effective depth of the substrate is smaller and the wall therefore appears relatively stiff. This, then, explains the sigmoid shape of the instability envelopes for the double-layer walls. Lastly, it is noted from Fig. 7 that, for a given plate flexural rigidity, the lower values of the substrate shear modulus give the lower growth rates of TSW. This suggests that, when investigating the TSW for points in the γ_s-$\bar{G}_s$ plane of Fig. 5, the best compliant-wall perfomance for a given plate flexural rigidity is found at the lower limit of $\bar{G}_s$ set by the divergence instability.

Figure 8 shows the effect of the upper-layer stiffness on the local amplitude of the TSW. Each result has been evaluated for the combination of substrate damping and shear modulus which gives the best performance regarding TSW and leaves the wall free from TWF and divergence up to a Reynolds number of 5750. Each pair of lines corresponds to a single value of the plate flexural rigidity, $\bar{B}_p$. The differences between the individual lines forming a pair stem from the manner in which $\bar{B}_p$ is constituted from the elastic modulus and thickness of the plate [recall that $B_p = E_p b^3/12(1-\nu_p^2)$]. Note that for a smaller b (with commensurately higher E_p) a lower substrate damping is required to suppress the TWF. This reduced damping aids the reduction of TSW growth rates, but the accompanying lower inertia of the upper layer exercises a deleterious effect on the TSW. However, it appears that these contrasting effects nearly cancel each other. Thus, it is seen that the single parameter, $\bar{B}_p$, represents a good characterization of the upper-layer properties. Nevertheless, for a given flexural rigidity it would be marginally preferable to use a very thin plate with a very high elastic modulus.

Turning to the effect of the upper-layer flexural rigidity in Fig. 8, it is evident that the flexural rigidity dictates the value of the initial maximum in the local amplitude of the TSW growth rates. The larger the flexural rigidity the larger the maximum. However, it is also seen that the larger values of flexural rigidity give lower values of the local amplitude at higher Reynolds numbers. To avoid transition, according to our conservative criterion, the local maximum must not exceed an amplification ratio of e^7. Therefore, the optimal flexural rigidity is that for which the initial maximum of the local amplitude is e^7. This in turn yields the largest range of Reynolds numbers in which the local amplitude does not exceed e^7.

Figure 9 summarizes the effect of upper-layer damping. In an analogous manner to Eq. (2), this can be introduced by setting $E_p = E_{pR}(1 - i\gamma_p)$, in Eqs. (10) where γ_p is the upper-layer damping coefficient. Each curve has been obtained by carrying out an optimization procedure which, following the previous discussions, places the local maximum of the TSW growth-rate envelope at e^7 and thus yields the maximum transition delay for the particular value of damping (and substrate depth). Increasing the upper-layer damping reduces the optimal value of the upper-layer flexural rigidity, thereby increasing the substrate stiffness required to prevent divergence, and consequently reducing the substrate damping needed for postponing the critical Reynolds number for the TWF to a value of 5750. The optimal properties of both upper and lower layers, for each value of γ_p, are presented in Table 1. Following the discussions above, the effect of the upper-layer stiffness can be closely characterized by the single parameter $\bar{B}_p$ (as shown in the

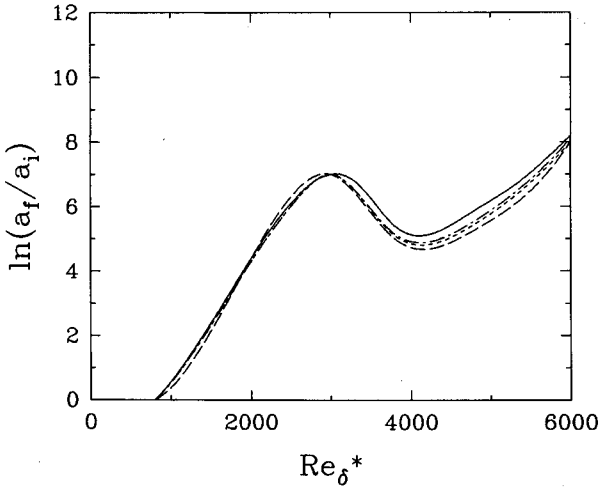

Fig. 9 Effect of upper-layer damping, gp on the maximum amplification envelopes for TSW, $\bar{d}$ = 1.80 throughout; for each γ_p, the remaining wall properties are optimised for maximum transition delay and presented in Table 1: ———, γ_p = 0.000;— · —, γ_p = 0.025; — — —, γ_p = 0.050; — —, γ_p = 0.075.

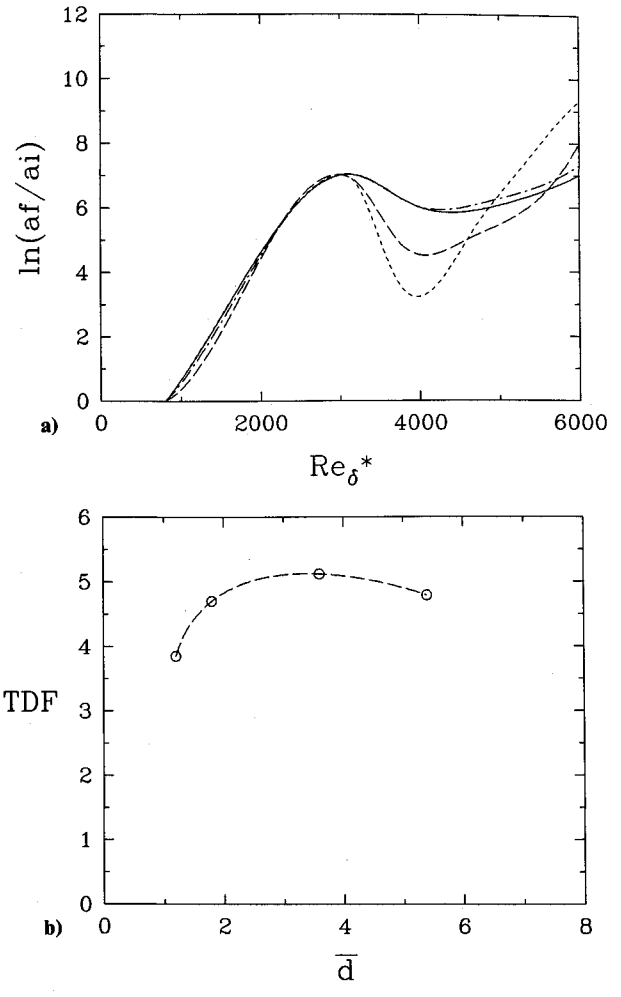

Fig. 10 Optimized double-layer walls: the effect of substrate thickness; for each case the wall has been optimized (with respect to all the other wall properties) such that TWF is stable up to the given $(Re_{\delta*})_{tr}$ and has marginal stability for divergence: a) Maximum amplification envelopes for TSW; for each case $\bar{b}$ = 0.12 and γ_p = 0.075: — — —, $\bar{d}$ = 1.2, $(Re\delta^*)_{tr}$ = 5200 with $\bar{G}_s$ = 0.329, γ_s = 0.0061, $\bar{B}_p$ = 0.01900; — —, $\bar{d}$ = 1.8, $(Re\delta^*)_{tr}$ = 5750 with $\bar{G}_s$ = 0.412, γ_s = 0.0152, $\bar{B}_p$ = 0.01824; ——, $\bar{d}$ = 3.6, $(Re_{\delta*})_{tr}$ = 6000 with $\bar{G}_s$ = 0.477, γ_s = 0.0153, $\bar{B}_p$ = 0.01732; — · —, $\bar{d}$ = 5.4, $(Re_{\delta*})_{tr}$ = 5800 with $\bar{G}_s$ = 0.491, γ_s = 0.0125, $\bar{B}_p$ = 0.01728 and b) transition-delay factor (TDF) vs wall thickness, data as above.

Table 1 Optimal properties for a double-layer wall with $\bar{d} = 1.8$

γ_p	$\bar{B}_p$	$\bar{G}_s$	γ_s
0.000	0.0239	0.400	0.028
0.025	0.0220	0.400	0.023
0.050	0.0200	0.405	0.019
0.075	0.0181	0.412	0.015

table). Nevertheless, it is noted that to generate these values we have used $\bar{b} = 0.1200$.

Note that in Fig. 9, the overall performance of the compliant wall is slightly improved by effectively locating as much of the required damping in the upper rather than the lower layer. For this wall depth, then, it is possible to attain a maximum transitional Reynolds number of 5700.

In all of the above results we have been working with a fixed wall thickness, $\bar{d} = 1.8$. To determine the absolute maximum transitional delay achievable using a double-layer wall, all of the above steps have been repeated for a set of different wall thicknesses. The results of this procedure are presented in Figs. 10a and 10b. It can be seen that the optimal nondimensional substrate thickness is approximately 3, although there is little difference between the values of 1.5–5. A very shallow substrate results in an effectively stiffer wall for large Reynolds numbers. However, if the wall is too deep, the prevention of divergence instability demands a relatively high value of the substrate shear modulus. The effective stiffness of the wall in these two extreme cases accounts for the existence of an optimal wall thickness. As can be seen from Fig. 10, it appears to be theoretically possible to delay transition up to a Reynolds number of 6000. In terms of distance along the wall, this represents a five-fold improvement on the performance of a rigid wall. This is somewhat better than, but comparable to, the best performance for the plate-spring compliant wall.[11,26] Consequently the estimates made in Ref. 26 of drag coefficients for various values of overall Reynolds number apply reasonably well to the optimum double-layer walls.

V. Conclusions

A highly efficient method has been developed for the prediction of Tollmien-Schlichting waves developing in a flate-plate boundary layer over a compliant wall. Spectral methods are used to obtain a matrix formulation of the coupled Orr-Sommerfeld/compliant-wall eigenproblem which can be solved rapidly on an SIMD parallel computer. The compliant wall may comprise either a single viscoelastic layer or two viscoelastic layers in which a relatively stiff, thin layer is supported by a much softer, thicker substrate. The second type of wall holds much promise for the postponement of transition and achieving drag reduction as evidenced by the successful experiments of Refs. 14–16. Methods for the prediction of the hydroelastic instabilities, TWF and divergence, which may occur in the wall/flow system are presented and discussed. These methods have been especially tailored for the particular instability and thus provide solutions extremely quickly. All three methods of instability prediction have been used together to carry out a wide parametric investigation of wall properties. Both single- and double-layer walls have been optimized in order to achieve maximum transition delay. The most important findings from the investigation are as follows:

1) For a single-layer compliant wall of sufficient thickness, there exists an optimal combination of shear modulus and wall damping. TWF is totally eliminated in this case. With this configuration, transition can be delayed by a factor of 2.5 over the rigid-wall result. The optimal performance is relatively insensitive to changes in thickness away from the effectively infinite depth value.

2) For both single- and double-layer walls, wall damping is desirable for, although in itself detrimental to TSW suppression, the reduction to the substrate stiffness that it permits (while maintaining marginal stability for TWF) results in an overall benefit for the reduction of TSW growth rates.

3) For double-layer walls, the optimum transition-delaying performance of the compliant wall is largely insensitive to the location of the wall damping, although the optimal structural parameters of both upper and lower layers are weakly dependent on the distribution of damping between the two layers. It appears to be marginally more desirable to locate as much of the wall damping as possible in the upper layer.

4) The key parameter for the upper-layer characterization is the flexural rigidity. For a given flexural rigidity, different combinations of elastic modulus and plate thickness have little effect on the TSW growth-rate envelopes.

5) A stiff upper layer behaves like a rigid wall at low Reynolds numbers but appears increasingly compliant at higher Reynolds numbers. In contrast, for a wall of given thickness, the effective compliance of the substrate decreases with increasing Reynolds numbers.

6) In the case of double-layer walls there exists an optimal value of the wall thickness. If this is used in combination with the optimal values of all the other lower- and upper-layer wall properties, then transition can be delayed by a factor of 5 times the rigid-wall result. This is slightly better than the best performance predicted for a plate-spring compliant wall.[11,26]

The last item details the best performance that can be achieved using a continuous isotropic double-layer compliant wall. Apart from exploiting anisotropic wall compliance (following the promising results of Yeo[18] and Carpenter and Morris,[11] which may pose manufacturing problems, improved performances may also be achieved by designing an optimized multipanel wall. For plate-spring compliant walls, this design strategy has been shown to be successful.[26] It is quite likely that similar results would be obtained using the present two-layer walls. Moreover arrays of smaller compliant panels have been shown to be significantly less susceptible to hydroelastic instability than one large panel.[42] This strategy warrants further investigation. Further work towards the practical implementation of compliant walls should address such issues as the influence of a mean pressure gradient on a coated body with curvature and aspects of the receptivity problem. Lastly, it is now known[48,49] that for compliant walls with good transition-delaying properties three-dimensional Tollmien-Schlichting waves grow more rapidly than two-dimensional waves. It could, therefore, be argued that the optimization procedure should be based on calculations of three-dimensional disturbances. This would be a daunting prospect computationally. Fortunately, Joslin et al.[48] have shown that the two-dimensional e^n calculations are not greatly in error and that the dominance of three-dimensional waves can be almost completely suppressed by using an orthotropic plate as the upper layer.

Appendix

The interfacial boundary conditions, Eqs. (9a and 9b), are

$$A_{01}\phi + A_{11}\phi' + A_{21}\phi'' = \Delta_{21} \quad \text{and} \quad A_{02}\phi + A_{12}\phi' + A_{32}\phi''' = \Delta_{22}$$

where

$$A_{01} = \mu\bar{\alpha}(\beta_{11}\beta_{32} - \beta_{31}\beta_{12})/\bar{\omega} + \bar{U}'\bar{\alpha}A_{11}/\bar{\omega} - \bar{\alpha}^2/Re_{\delta*}$$

$$A_{11} = i\mu(\beta_{41}\beta_{12} - \beta_{42}\beta_{11})/\bar{\omega}, \qquad A_{21} = -1/Re_{\delta*}$$

$$A_{02} = \mu\bar{\alpha}(\beta_{32}\beta_{21} - \beta_{31}\beta_{22})/\bar{\omega} + \bar{U}'(1 + \bar{\alpha}D/\bar{\omega})$$

$$A_{12} = D + \bar{\omega}/\bar{\alpha} + 3i\bar{\alpha}/Re_{\delta*}, \qquad A_{32} = -i/(\bar{\alpha}Re_{\delta*})$$

$$D = i\mu(\beta_{22}\beta_{41} - \beta_{21}\beta_{42})/\bar{\omega}, \qquad \mu = (\beta_{32}\beta_{41} - \beta_{31}\beta_{42})^{-1}$$

and where

$$\beta_{11} = \bar{G}_s[2_i\bar{\alpha}f_t\xi_{11} - (\bar{\alpha}^2 + f_t^2)\xi_{12}]$$

$$\beta_{12} = \bar{G}_s[(\bar{\alpha}^2 + f_t^2)\,\xi_{21} + 2i\bar{\alpha}f_t\xi_{22}]$$

$$\beta_{21} = \bar{G}_s(\bar{\alpha}^2 + f_t^2)\,(2 - \xi_{11}) - 2i\bar{\alpha} f_t \xi_{12}$$

$$\beta_{22} = -\,\bar{G}_s[(\bar{\alpha}^2 + f_t^2)\,\xi_{22} - 2i\bar{\alpha} f_t (2 + \xi_{21})]$$

$$\beta_{31} = i\bar{\alpha}(2 - \xi_{11}) + f_t \xi_{12}, \qquad \beta_{32} = -\,i\bar{\alpha}\xi_{22} - f_t(2 + \xi_{21})$$

$$\beta_{41} = f_l \xi_{11} + i\bar{\alpha}\xi_{12}, \qquad \beta_{42} = f_l \xi_{22} - i\bar{\alpha}\xi_{21}$$

$$\xi_{11} = 1 + \frac{\bar{\alpha}^2 + f_l f_t}{\bar{\alpha}^2 - f_l f_t} e^{-2f_t\bar{h}}, \qquad \xi_{12} = \frac{2i\bar{\alpha} f_l}{\bar{\alpha}^2 - f_l f_t} e^{-(f_l + f_t)\bar{h}}$$

$$\xi_{21} = -1 + \frac{\bar{\alpha}^2 + f_l f_t}{\bar{\alpha}^2 - f_l f_t} e^{-2f_t\bar{h}}, \qquad \xi_{22} = \xi_{12}\frac{f_t}{f_l}$$

$$f_t = (\bar{\alpha}^2 - C_{m2}\bar{\omega}^2/\bar{G}_s)^{1/2}, \qquad f_l = [\bar{\alpha}^2 - C_{m2}\bar{\omega}^2/(\bar{K}_s + 4\bar{G}_s/3)]^{1/2}$$

The term $\bar{U}'$ is the derivative of the Blasius velocity profile evaluated at the undisturbed interface $\bar{z} = 0$ and C_{m2} is the relative density of the substrate. Working from Eqs. (10a) and (10b), appropriate expressions for the stress contribution due to the thin upper layer at $\bar{z} = 0$ are

$$\Delta_{21} = -i\frac{i\bar{b}}{\bar{\omega}}\,(\bar{E}_p\bar{\alpha}^2 - C_{m1}\omega^2)\,(\phi' + \bar{U}'\bar{\alpha}\phi/\bar{\omega})$$

$$\Delta_{22} = -\,\frac{\bar{\alpha}}{\bar{\omega}}\,(\alpha^{-4}\bar{B}_p\bar{b}^2 - C_{m1}\bar{b}\bar{\omega}^2)\,\phi$$

where $\bar{E}_p$, $\bar{B}_p$, $\bar{b}$, and C_{m1} are, respectively, the elastic modulus, flexural rigidity, thickness, and relative density of the plate. In all of the preceding calculations, the densities of the three media have been taken to be identical. The terms $\bar{U}'$ and ϕ are evaluated at $\bar{z} = 0$ in the preceding expressions.

Acknowledgment

This work is part of a research program at the University of Warwick which was supported by the Ministry of Defence (Procurement Executive).

References

[1]Kramer, M. O., "Boundary-Layer Stabilization by Distributed Damping," *Journal of the American Society of Naval Engineers*, Vol. 72, Feb. 1960, pp. 25-33; *Journal of the Aero/Space Sciences*, Vol. 27, Jan. 1960, p. 69.

[2]Kramer, M. O., "Boundary-Layer Stabilization by Distributed Damping," *Journal of the American Society of Naval Engineers*, Vol. 74, May 1962, pp. 341–348.

[3]Benjamin, T. B., "Effects of a Flexible Boundary on Hydrodynamic Stability," *Journal of Fluid Mechanics*, Vol. 9, Pt. 4, 1960, pp. 513–532.

[4]Benjamin, T. B., "The Threefold Classification of Unstable Disturbances in Flexible Surfaces Bounding Inviscid Flows," *Journal of Fluid Mechanics*, Vol. 16, Pt. 3, 1963, pp. 436–450.

[5]Landahl, M. T., "On the Stability of a Laminar Incompressible Boundary Layer over a Flexible Surface," *Journal of Fluid Mechanics*, Vol. 13, Pt. 4, 1962, pp. 609–632.

[6]Landahl, M. T., and Kaplan, R. E., "Effect of Compliant Walls on Boundary Layer Stability and Transition," AGARDograph 97-1-353, 1965.

[7]Bushnell, D. M., and Hefner, J. N., "Effect of Compliant Wall Motion on Turbulent Boundary Layers," *Physics of Fluids*, Vol. 20, No. 10, Pt. II, Oct. 1977, pp. S31–S48.

[8]Carpenter, P. W., and Garrad, A. D., "The Hydrodynamic Stability of Flows over Kramer-Type Compliant Surfaces. Pt. 1. Tollmien-Schlichting Instabilities," *Journal of Fluid Mechanics*, Vol. 155, June 1985, pp. 465–510.

[9]Carpenter, P. W., and Garrad, A. D., "The Hydrodynamic Stability of Flows over Kramer-Type Compliant Surfaces. Pt. 2. Flow-Induced Surface Instabilities," *Journal of Fluid Mechanics*, Vol. 170, Sept. 1986, pp. 199–232.

[10]Carpenter, P. W., Gaster, M., and Willis, G. J. K., "A Numerical Investigation into Boundary Layer Stability on Compliant Surfaces," *Numerical Methods in Laminar and Turbulent Flow*, Pineridge, Swansea, Wales, UK, Aug. 1983, pp. 166–172.

[11]Carpenter, P. W., and Morris, P. J., "The Effect of Anisotropic Wall Compliance on Boundary-Layer Stability and Transition," *Journal of Fluid Mechanics*, Vol. 218, Sept. 1990, pp. 171–223.

[12]Duncan, J. H., Waxman, A. W., and Tulin, M. P., "The Dynamics of Waves Between a Visco-Elastic Coating and a Fluid Flow," *Journal of Fluid Mechanics*, Vol. 158, Sept. 1985, pp. 177–197.

[13]Fraser, L .A., and Carpenter, P. W., "A Numerical Investigation of Hydroelastic and Hydrodynamic Instabilities in Laminar Flows over Compliant Surfaces Comprising One or Two Layers of Visco-Elastic Material," *Numerical Methods in Laminar and Turbulent Flow*, Pineridge, Swansea, Wales, UK, July 1985, pp. 1171–1181.

[14]Daniel, A. P., Gaster, M., and Willis, G. J. K., "Boundary Layer Stability on Compliant Surfaces," British Maritime Technology Ltd., Final Rept. No. 35020, Teddington, England, UK, April 1987.

[15]Gaster, M., "Is the Dolphin a Red Herring?," *Proceedings of the International Union of Theoretical and Applied Mechanics Symposium on Turbulence Management and Relaminarisation* (Bangalore, India), edited by H. W. Liepmann and R. Narasimha, Springer, New York, Jan. 1987, pp. 285–304.

[16]Willis, G. J. K., "Hydrodynamic Stability of Boundary Layers over Compliant Surfaces," Ph.D. Thesis, University of Exeter, School of Engineering, England, UK, June 1986.

[17]Yeo, K. S., "The Stability of Boundary-Layer Flow over Single- and Multi-Layer Viscoelastic Walls," *Journal of Fluid Mechanics*, Vol. 196, Nov. 1988, pp. 359–408.

[18]Yeo, K. S., "The Hydrodynamic Stability of Boundary-Layer Flow over a Class of Anisotropic Compliant Walls," *Journal of Fluid Mechanics*, Vol. 220, Nov. 1990, pp. 125–160.

[19]Metcalfe, R. W., Battistoni, F., Orszag, S. A., and Ekeroot, J., "Evolution of Boundary Layer Flow over a Compliant Wall During Transition to Turbulence," *Proceedings of Conference on Boundary Layer Transition and Control* (Cambridge, UK), Royal Aeronautical Society, London, April 1991, pp. 36.1–36.14.

[20]Sen, P. K., and Arora, D. S., "On the Stability of Laminar Boundary-Layer Flow over a Flat-Plate with a Compliant Surface," *Journal of Fluid Mechanics*, Vol. 197, Dec. 1988, pp. 201–240.

[21]Riley, J. J., Gad-el-Hak, M., and Metcalfe, R. W., "Compliant Coatings," *Annual Review of Fluid Mechanics*, Vol. 20, 1988, pp. 393–420.

[22]Gad-el-Hak, M., "Boundary Layer Interactions with Compliant Coatings: An Overview," *Applied Mechanics Review*, Vol. 39, No. 4, April 1986, pp. 511–524.

[23]Carpenter, P. W., "Status of Transition Delay Using Compliant Walls," *Viscous Drag Reduction in Boundary Layers*, edited by D. M. Bushnell and J. N. Heffner, Vol. 123, *Progress in Astronautics and Aeronautics*, AIAA, Washington, DC, 1990, pp. 79–113.

[24]Carpenter, P. W., "The Optimization of Compliant Surfaces for Transition Delay," University of Exeter, School of Engineering, TN 85/2, Exeter, England, UK, Oct. 1985.

[25]Carpenter, P. W., "The Optimization of Compliant Surfaces for Transition Delay," *Proceedings of the International Union of Theoretical and Applied Mechanics Symposium on Turbulence Management and Relaminarisation* (Bangalore, India), edited by H. W. Liepmann and R. Narasimha, Springer, New York, Jan. 1987, pp. 305–313.

[26]Carpenter, P. W., "The Optimization of Multiple-Panel Compliant Walls for Delay of Laminar-Turbulent Transition," *AIAA Journal*, Vol. 31, No. 7, 1993, pp. 1187–1188.

[27]Lucey, A. D., and Carpenter, P. W., "A Numerical Simulation of the Interaction of a Compliant Wall and Inviscid Flow," *Journal of Fluid Mechanics*, Vol. 234, Jan. 1992, pp. 121–146.

[28]Lucey, A. D., and Carpenter, P. W., "A study of the Hydroelastic Stability of a Compliant Panel Using Numerical Methods," *International Journal of Numerical Methods in Heat and Fluid Flow*, Vol. 2, Dec. 1992, pp. 537–553.

[29]Hansen, R. J., and Hunston, D. L., "An Experimental Study of Turbulent Flows over Compliant Surfaces," *Journal of Sound and Vibration*, Vol. 34, No. 3, 1974, pp. 297–308.

[30]Hansen, R. J., and Hunston, D. L., "Fluid-Property Effects on Flow-Generated Waves on a Compliant Surface," *Journal of Fluid Mechanics*, Vol. 133, Aug. 1983, pp. 161–177.

[31]Gad-el-Hak, M., Blackwelder, R. F., and Riley, J. J., "On the Interaction of Compliant Coatings with Boundary-Layer Flows," *Journal of Fluid Mechanics*, Vol. 140, Mar. 1984, pp. 257–280.

[32]Carpenter, P. W., "The Effect of a Boundary Layer on the Hydroelastic Instability of Infinitely Long Plates," *Journal of Sound and Vibration*, Vol. 93, No. 3, 1984, pp. 461–464.

[33]Lucey, A. D., Carpenter, P. W., and Dixon, A. E., "The Role of Wall Instabilities in Boundary-Layer Transition over Compliant Walls," *Pro-*

ceedings of Conference on Boundary Layer Transition and Control (Cambridge, UK)Royal Aeronautical Society, London, England, April 1991, pp. 35.1–35.10.

[34]Gyorgyfalvy, D., "Possibilities of Drag Reduction by the Use of a Flexible Skin," *Journal of Aircraft*, Vol. 4, Feb. 1967, pp. 186–192.

[35]Carpenter, P. W., and Gajjar, J. S. B., "A General Theory for Two- and Three-Dimensional Wall-Mode Instabilities in Boundary Layers over Isotropic and Anisotropic Compliant Walls," *Theoretical and Computational Fluid Dynamics*, Vol. 1, No. 6, 1990, pp. 349–378.

[36]Canuto, C., Hussaini, M. Y., Quarteroni, A., and Zang, T. A., *Spectral Methods in Fluid Dynamics*, Springer, New York, 1988.

[37]Bridges, T. J., and Morris, P. J., "Differential Eigenvalue Problems in which the Parameter Appears Nonlinearly," *Journal of Computational Physics*, Vol. 55, No. 3, 1984, pp. 437–460.

[38]Jordinson, R., "The Flat Plate Boundary Layer. Pt. 1. Numerical Integration of the Orr-Sommerfeld Equation," *Journal of Fluid Mechanics*, Vol. 43, Pt. 4, 1970, pp. 801–811.

[39]Yeo, K. S., "The Stability of Flow over Flexible Surfaces," Ph.D. Thesis, Dept. of Engineering, Univ. of Cambridge, UK, Nov. 1986.

[40]Kendall, J. M., "The Turbulent Boundary Layer over a Wall with Progressive Waves," *Journal of Fluid Mechanics*, Vol. 41, Pt. 2, 1970, pp. 259–281.

[41]Balasubramanian, R., and Orszag, S. A., "Numerical Studies of Laminar and Turbulent Drag Reductions," NASA CR 3669, 1983.

[42]Lucey, A. D., and Carpenter, P. W., "The Hydroelastic Stability of Three-Dimensional Disturbances of a Finite Compliant Panel," *Journal of Sound and Vibration*, Vol. 163, No. 3, 1993, pp. 527–552.

[43]Werle, J., Lucey, A. D., and Carpenter, P. W., "Hydroelastic Instability of Compliant Walls Using the Finite-Element Method," *Numerical Methods in Engineering* 92, Elsevier, Amsterdam, The Netherlands, Sept. 1992, pp. 765–772.

[44]Smith, A. M. O., and Gamberoni, H., "Transition Pressure Gradient and Stability Theory," Douglas Aircraft Co., Rept. ES 26388, Long Beach, CA, Aug. 1956.

[45]Joslin, R. D., and Morris, P. J., "Effect of Compliant Walls on Secondary Instability in Boundary-Layer Transition," *AIAA Journal*, Vol. 30, No. 2, 1992, pp. 332–339.

[46]Thomas, M. D., "On the Resonant Triad Interaction over Rigid and Flexible Boundaries," *Journal of Fluid Mechanics*, Vol. 234, Jan. 1992, pp. 417–441.

[47]Thomas, M. D., "The Non-Linear Stability of Flows over Compliant Walls," *Journal of Fluid Mechanics*, Vol. 239, June 1992, pp. 657–670.

[48]Joslin, R. D., Morris, P. J., and Carpenter, P. W., "The Role of Three-Dimensional Instabilities in Compliant-Wall Boundary-Layer Transition," *AIAA Journal*, Vol. 29, No. 10, 1991, pp. 1603–1610.

[49]Yeo, K. S., "The Three-Dimensional Stability of Boundary-Layer Flow over Compliant Walls," *Journal of Fluid Mechanics*, Vol. 238, May 1992, pp. 537–577.